J. Fluid Mech. (1998), *vol.* 365, *pp.* 109–136. Printed in the United Kingdom

© 1998 Cambridge University Press

Spray jets in a cross-flow

By S. GHOSH AND J. C. R. HUNT

Department of Applied Mathematics and Theoretical Physics, University of Cambridge, Silver Street, Cambridge CB3 9EW UK

(Received 21 May 1997 and in revised form 14 January 1998)

When droplets are expelled at a high velocity by a spray, a strong vertical air jet is induced throughout which the smallest droplets are dispersed (their Reynolds numbers associated with their relative motion being small). In our analysis we focus on the interaction between an external cross-flow and this spray jet. This interaction and the distances by which the spray jet and, over a longer distance, the large droplets are deflected are found to depend largely on the ratio of the cross-wind speed to the induced air speed U_0/U_j. Using a multi-zone analysis we show that with a weak cross-flow ($U_0/U_j \lesssim 0.1$), in the region immediately below the nozzle the spray entrains the external cross-flow and acts like a line sink; the streamlines close to the spray curve inwards to the centre, while further away the sink flow is weak and the streamlines follow the cross-wind. The external flow stagnates at a certain distance from the spray centreline which depends on U_0/U_j. When $U_0/U_j \gtrsim 0.1$ the cross-section of the spray jet and its velocity distribution change in the same way as a fluid jet in a cross-flow, whose inertia causes the deflection of the external flow around it and whose surface vorticity causes a pair of axial vortices on the downwind side of the spray. These vortices have a significant effect on the spray because they induce a back flow which reduces the tendency of the small droplets to leave the spray. When the cross-wind is strong ($U_0/U_j > 0.3; U_0 \gtrsim 10$ m s^{-1}) the flow is too strong to be entrained; in this limit the main effect of the larger spray droplets is simply to resist the cross-flow which causes the cross-flow to slow down as it passes through the spray and to divert some of the cross-flow around the spray jet. Since the cross-flow now passes through the spray it carries the smallest droplets downwind.

In this paper analytical models have been developed for all the practical ranges of the ratio of the jet speed to the cross-wind speed. This enables spray drift to be calculated. These models require very little computer time and can be run interactively. Spray droplet trajectories can be plotted straightforwardly for both axisymmetric and flat-fan sprays.

1. Introduction

When agricultural sprays are used to apply chemicals to crops the sprays are generally carried on booms which are moved over the crops behind a tractor (figure 1). The high velocity of the droplets in the spray induces a strong vertical air flow with an initial velocity of about 20 m s^{-1}, which disperses the smallest droplets throughout the jet. The forward movement of the tractor induces a relative cross-wind (typically with velocities U_{x0} in the range of 3 to 5 m s^{-1}), which together with any natural wind (with velocity U_{y0} that in practice has to be less than U_{x0}), affects the spray in two ways, first, by bending over and distorting the vertical air jet induced by the spray and secondly, by deflecting the larger droplets. The first effect leads to the

https://doi.org/10.1017/S0022112098001190 Published online by Cambridge University Press

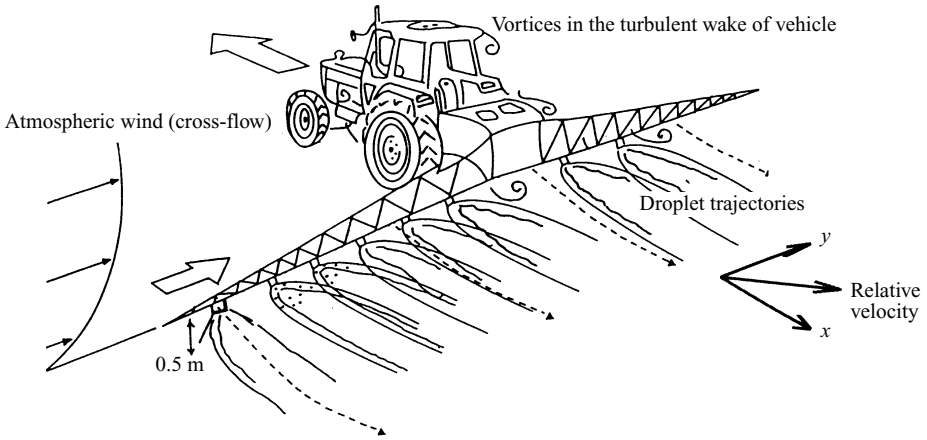


FIGURE 1. Diagram of agricultural sprays drawn by a tractor moving at a speed U_{x0} in a cross-flow with velocity U_{y0}.

smallest droplets escaping from the spray and therefore not impinging directly on to the crops. Furthermore, by escaping into the atmosphere downwind of the spray, although they are dispersed by the atmospheric turbulence, their concentration may be great enough to cause an environmental hazard, commonly termed 'spray drift'. A detailed understanding of the fluid mechanics of sprays in cross-winds is necessary to improve the design and operating procedures for sprays (for example deciding on the appropriate spray height and the speed of the tractor supporting the spray) and also to improve the calculation of the downwind transport of light spray particles (in particular determining the flux and size distribution and the effective height at which particles of different diameters escape from the spray into the cross-flow).

We have found no previous detailed studies of the fluid mechanics of sprays in cross-flows. However there have been several calculations of dispersion downwind of sprays (Miller & Hadfield 1988; Walklate 1987) which had to be based on several assumptions about the source 'strength' of the plume of dispersing droplets (see also Fuchs 1964; Bache & Johnstone 1992). There are other technological and many natural processes, including rain clouds and volcanoes, where wide distributions of size of particles and droplets are ejected at relatively high speeds into cross-flows.

Previous research investigations that are relevant to the problem are those on sprays in still air. Ghosh & Hunt (1994) in their review explained how the induced air flows in spray jets have many similarities with the air flow in turbulent jets, and can be analysed using concepts and models first proposed by Morton, Taylor & Parker (1956). However, Ghosh, Phillips & Perkins (1991) also showed that there are some important differences between these two kinds of jets both in the structure of turbulence – the eddy scales are much smaller in a spray jet because of the wakes of the droplets – and in the mean flow – the extra momentum provided to the air flow leads to a slower decay of the speed of the induced air in the spray jet compared with a typical gas jet.

In this paper we begin our study of the effects of a cross-flow on a spray jet by considering how fluid jets are deflected and deformed by cross-flows, a fundamental problem in fluid mechanics that is still not fully understood. For very weak cross-flows we base our model on the original work of G. I. Taylor (1958) and the more recent theoretical and experimental study by Coelho & Hunt (1989). For stronger

https://doi.org/10.1017/S0022112098001190 Published online by Cambridge University Press

cross-flows, which penetrate the spray jet, a different approach is necessary; this is based on an analysis of the deflection of the cross-flow caused by the drag of the droplets in the spray. (Our studies here show how this varies considerably with the angle of the spray and whether it is axisymmetric or a 'flat-fan' spray). To model the latter process we apply the analysis by G. I. Taylor (1944) of air flow through a gauze.

The very large velocity gradients around single-phase jets in cross-flows cannot be completely resolved even by the largest possible number of grid points (at least 32^3) on three-dimensional meshes on large computers (e.g. Sykes, Lellewen & Parker 1986). Spray jets would require even more computer time because the solutions are needed for many coupled equations corresponding to different ranges of particle sizes (Crowe, Sharma & Stock 1977). To avoid this complexity and expense and to provide models that can be adapted and understood by those not expert in computational fluid dynamics, we have developed analytical models in which the results are expressed in formulae or in easily computable first-order ordinary differential equations for the trajectories of the spray droplets.

2. Modelling of the main physical processes for a spray jet in an atmospheric cross-wind

2.1. *Mechanisms*

When a liquid first emerges through a pressure atomizing nozzle it is in the form of a jet or a sheet which quickly disintegrates into droplets due to aerodynamic instabilities in the 'break up region' which interact strongly with the atmosphere. Just downstream in the 'spray region', the liquid is only in the form of droplets. Considerable effort has been directed towards the investigation of the break-up region and just beyond (Dombrowski & Johns 1963; Squire 1953; Dombrowski & Frazer 1953; Castleman 1931; Schweitzer 1937). On the other hand analyses of the behaviour of droplets further away are relatively scarce, especially in a cross-wind.

There are three important aspects of air flow and droplet movement in the spray region: (i) except very close to the source, vertical air motion is induced by the drag of the larger droplets; (ii) cross-flows which are caused by a cross-wind or by the motion of the vehicle change the air jet which leads first to the smaller and then the larger droplets being dragged out of the spray; (iii) subsequent downstream transport of the droplets by the wind and turbulence in the atmosphere.

The first of these processes has been described by us in an earlier paper (Ghosh & Hunt 1994), while the third process has been analysed by Walklate (1987). This paper focuses on stage (ii), which we describe as follows.

Where the vertical velocity of the air flow induced in the spray jet decreases away from the nozzle the induced flow becomes weaker in relation to the velocity of the cross-flow, and different dynamical processes operate at different distances from the nozzle. As in other complex turbulent flows, an analysis for the whole flow field can be constructed by considering different models for each of the different zones, labelled 𝔸 to 𝔻, in which different dynamical processes are dominant. Depending on the relative values of the cross-wind speed U_0 and the initial induced vertical air speed V_j in the jet, and on the distance along the jet that is being considered, these zones may be either negligibly small or non-existent in any particular case.

https://doi.org/10.1017/S0022112098001190 Published online by Cambridge University Press

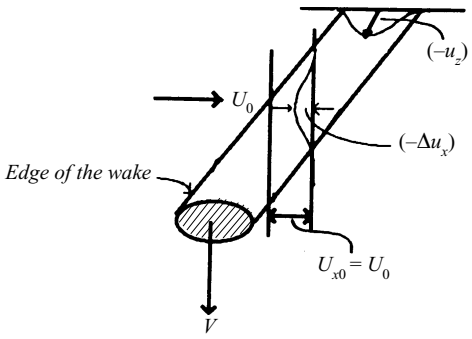


FIGURE 2. Schematic of the wake shape and instantaneous velocity profiles of the horizontal and vertical velocity components $(U_{x0} + \Delta u_x, u_z)$ behind a spray droplet moving downwards with a velocity V in a cross-flow U_0 in the x-direction.

2.2. *Effect of a cross-wind on flow around individual particles*

In order to understand how a spray in still air induces jet flow, it is necessary to analyse the force on the individual droplets which for simplicity are assumed to be spherical (Ghosh & Hunt 1994). In the same way a model for the effects of a cross-wind can be constructed from an analysis of the forces F_x, F_y, F_z on particles moving vertically with velocity V in a horizontal cross-flow (U_x, U_y).

If the drag coefficient is C_D, the drag force is

$$(F_x, F_y, F_z) = \tfrac{1}{2} C_D \rho \left[U_x, U_y, -V\right] \left[U^2 + V^2\right]^{1/2} \pi a^2, \tag{2.1}$$

where $U^2 = U_x^2 + U_y^2$; a is the droplet radius, and ρ is the air density. The drag coefficient is calculated from the widely used formulation given by Wallis (1969) (see equation (3.7) below).

For the smaller droplets $C_D \sim Re^{-1}$, where

$$Re = \left[a(U^2 + V^2)^{1/2}/\nu\right] , \tag{2.2}$$

in which case F_x, F_y are independent of V. But for larger droplets $C_D \sim 1$, and therefore, if $U/V \ll 1$ the horizontal drag forces are proportional to (U/V) times the vertical drag, and may be neglected.

The perturbation to the flow in the wake of each droplet is proportional to $\boldsymbol{F}$ (Batchelor 1967, p. 349). In a cross-wind the wakes of the particles are swept to the downwind side of the particle, and therefore not only do the particles induce a downward motion (u_z) in their wakes, but they induce a deficit $(-\Delta u_x)$ in the horizontal wind speed (see figure 2). As in the case of a spray in still air, the net effect of many wakes on the air flow is obtained by considering the net force on the air induced by the particles. (For a detailed discussion see Hunt, Perkins & Fung 1994.)

When (2.1) is used to calculate the horizontal force on the particles the horizontal wind speed is not necessarily equal to the external or far-field values of U_x, U_y $(= U_{x0}, U_{y0})$. The reason is that when $U_0 = (U_{x0}^2 + U_{y0}^2)^{1/2}$ is much less than the droplet speed V, the vertical air jet induced by the droplets (with velocity U_j) induces significant horizontal motions (U_x, U_y) (of the order of the entrainment velocity U_e). Since these can be as large as U_0, in this case the horizontal induced air motion is primarily determined by the vertical force on the droplets, and not the horizontal drag force!

https://doi.org/10.1017/S0022112098001190 Published online by Cambridge University Press

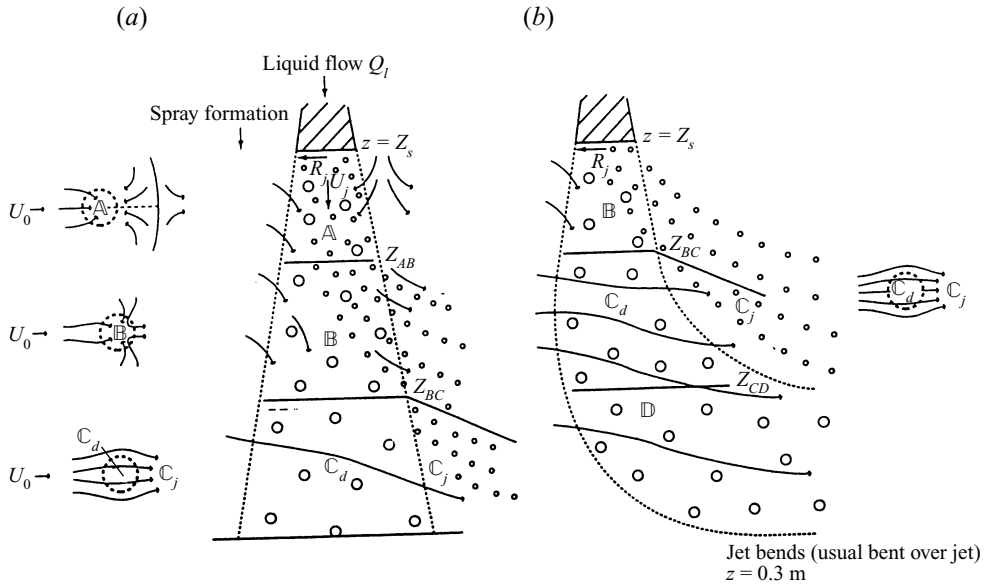


FIGURE 3. Flow zones for a spray jet in cross-flow (without any ground effect) with typical flow zones corresponding to different ratios of the entrainment velocity U_e, jet speed U_j, cross-flow U_0, and droplet speed V. (*a*) Weak cross-wind ($U_0 \leqslant U_e$); horizontal cross-section and vertical cross-sections. (*b*) Moderate cross-wind ($U_0 > U_e$) (strong cross-wind where ($U_0 > U_e \approx V$) is not shown!). Zone $\mathbb{A}$: air entrained; ($U_j > U_e > U_0$). Zone $\mathbb{B}$: air entrained, small droplets dispersed downwind; $V > U_j > U_0 > U_e$. Zone $\mathbb{C}$: all air passes through spray, small droplets dispersed; $V > U_0 > U_j$ (two components $\mathbb{C}_d$, $\mathbb{C}_j$). Zone $\mathbb{D}$: even large drops dispersed; $U_0 \geqslant V \approx U_j$.

However, when U_0 is large compared to U_e, (2.1) can be applied to estimate the horizontal force on the droplets, with $U_x = U_{x0}$, $U_y = U_{y0}$. Note that the horizontal forces acting on many droplets produce variations in the distributed perturbation in the horizontal velocity which when averaged over a volume containing many droplets, certainly do not lead to simple straight line wakes, such as shown in figure 2! It is assumed in our analysis that the x-axis of the coordinates is taken parallel to the mean relative velocity at the spray jet. Interaction between spray jets is neglected. A full calculation is necessary as shown in § 2.3.

2.3. *Weak cross-wind ($U_0 \ll U_e$)*

If the cross-wind is weak ($\lesssim 1.0$ m s^{-1} for our spray problem), then the entrainment velocity (roughly a tenth of the air jet speed) is greater than the cross-wind speed (about 1.0 m s^{-1}). As a result the surrounding fluid is sucked in (Coelho & Hunt 1989; Taylor 1958), which means that the spray centreline acts like a line sink for the surrounding fluid. This is described in the analysis that follows and we refer to this flow zone as zone $\mathbb{A}$ which extends from the height Z_0, where the spray jet is fully formed to the level Z_{AB} where it joins region $\mathbb{B}$. See figures 3 and 4. The height Z_0 is below the level Z_s, where the spray jet is created (e.g. by a spray nozzle or the instability of a liquid jet).

The relative approach flow is exactly uniform when the spray is moved through still air. Even in a cross-wind, since the horizontal gradients in the external flow caused by the perturbed flow around the spray are of the order U_0/ℓ, these are generally much greater than the vertical shear of the cross-wind ($\partial U_0/\partial z$). Therefore in the external flow the velocity $\boldsymbol{u}$ can be assumed to be irrotational, so that $\boldsymbol{u} = -\nabla\phi$ where

https://doi.org/10.1017/S0022112098001190 Published online by Cambridge University Press

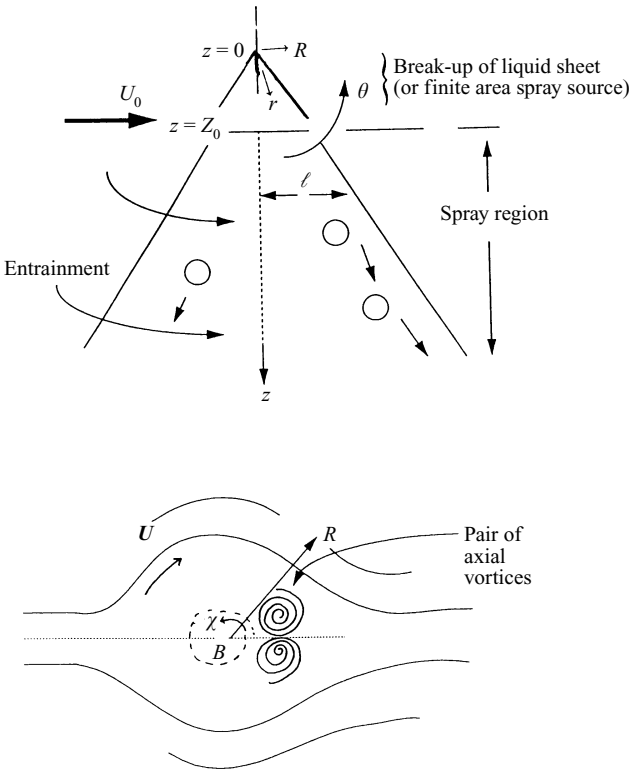


FIGURE 4. Schematic of the spray region entraining air and a plan view showing a pair of axial vortices downwind of the spray jet.

ϕ satisfies Laplace's equation

$$\nabla^2\phi = 0\ . \tag{2.3}$$

The boundary condition far away from the spray is

$$\text{as} \quad r \to \infty, \quad \boldsymbol{u} = (U_0, 0, 0)$$

i.e. the velocity tends to the uniform velocity U_0 , or in spherical coordinates,

$$\phi = U_0 r \sin\theta \cos\chi\ . \tag{2.4a}$$

At the outer edge of the spray (at a radial distance $r\sin\theta > l$ from the axis, where $l(r)$ is the effective radius of the jet at a distance r along the axis) it is assumed that the cross-flow is weak relative to the entrainment velocity (i.e. $v_\theta \gg U_0$). The external air flow is entrained into the spray at a rate $E(r)$ per unit axial distance, which is related to ϕ and angular velocity v_θ by the equation

$$\int_0^{2\pi} \frac{\partial\phi}{\partial\theta}\mathrm{d}\chi = E(r) = v_\theta\, 2\pi r \sin\theta. \tag{2.4b}$$

In other words $v_\theta \to U_e$ where U_e is the entrainment velocity. Above the jet ($\theta > \frac{1}{2}\pi$) the perturbation velocity field is continuous.

As usual with linear problems having two independent boundary conditions, it is convenient to consider the solution as the superposition of two solutions, namely

$$\nabla\phi = \nabla\phi_1 + \nabla\phi_2 \tag{2.5a}$$

https://doi.org/10.1017/S0022112098001190 Published online by Cambridge University Press

where $\nabla\phi_1$ corresponds to the velocity field around the spray jet caused by the uniform approach flow impinging onto an impervious body. The latter effect is equivalent to the formation of a vortex sheet around the jet as the external flow passes around it (Coelho & Hunt 1989). Therefore

$$\text{as} \quad r\sin\theta/l \to \infty, \quad \phi_1 \to U_0\, r\sin\theta\cos\chi \tag{2.5b}$$

and

$$\text{on} \quad r\sin\theta \simeq l, \quad \frac{\partial\phi_1}{\partial r} = 0. \tag{2.5c}$$

The second term $\nabla\phi_2$ corresponds to the perturbation in the external flow caused by the entrainment, so that ϕ_2 satisfies (2.4*b*), and as $r \to \infty$

$$|\,\nabla\phi_2\,| \to 0\,. \tag{2.5d}$$

Note that this solution is the first term in an asymptotic expansion in $\epsilon = U_0/U_e$. As the cross-flow increases the deformation of the jet has to be considered. (In § 2.4 we consider a different form of solution when ϵ is of the order unity.) ϕ_1 can be derived directly from (2.3). Since $l(r) \ll r$, it is more convenient to express (2.3), the blocking solution, locally in cylindrical polar coordinates (R, χ, z) where $R = r\sin\theta$, $z = r\cos\theta$ and $\chi = \sin^{-1} x/y$. Then (2.3) becomes

$$\frac{1}{R}\frac{\partial^2(R\phi_1)}{\partial r^2} + \frac{\partial^2\phi_1}{R^2\partial\chi^2} + \frac{\partial^2\phi_1}{\partial z^2} = 0\,. \tag{2.6a}$$

Since for the flow outside thin axisymmetric jets $r \gg l(r)$ (and $z \gg l(z)$), $\left(\partial^2\phi_1/\partial z^2\right)$ is negligible compared to the other terms. Then the blocking solution is, to first order, a local two-dimensional solution, namely

$$\phi_1 = U_0 R\cos\chi\left(1 + l^2/R^2\right), \tag{2.6b}$$

or in spherical polar coordinates

$$\phi_1 = U_0 r\sin\theta\cos\chi\left(1 + l^2(r)/\left(r^2\sin^2\theta\right)\right). \tag{2.6c}$$

This form of 'blocking' perturbation around a jet was verified experimentally by Coelho & Hunt (1989).

For the case of an axisymmetric spray in which the azimuthal dependence χ can be neglected, the external perturbation flow field caused by the blockage of the jet and by entrainment into the jet are also axisymmetric. ϕ_2 can most easily be analysed using Stokes' stream function $\psi(r, \phi)$ (Batchelor 1967, pp. 78–79, 450–451):

$$u_r = \frac{\partial\phi_2}{\partial r} = \frac{1}{r^2\sin\theta}\frac{\partial\psi\,(r,\theta)}{\partial\theta}\,, \quad u_\theta = \frac{1}{r}\frac{\partial\phi_2}{\partial\theta} = -\frac{1}{r\sin\theta}\frac{\partial\psi\,(r,\theta)}{\partial r}\,. \tag{2.7a}$$

Then equation (2.3) transforms to

$$\frac{\partial^2\psi}{\partial r^2} + \frac{1-\mu^2}{r^2}\,\frac{\partial^2\psi}{\partial\mu^2} = 0 \tag{2.7b}$$

where $\mu = \cos\theta$. The appropriate solution is

$$\psi = \frac{C}{n+1}r^{n+1}\left(1-\mu^2\right)\frac{\mathrm{d}P_n}{\mathrm{d}\mu}(\mu)\,, \tag{2.7c}$$

https://doi.org/10.1017/S0022112098001190 Published online by Cambridge University Press

whence from (2.7*a*) the angular velocity v_θ is given by

$$v_\theta = -Cr^{n-1}\sin\theta\frac{\mathrm{d}P_n(\mu)}{\mathrm{d}\mu}, \tag{2.8}$$

where C is a constant of integration, and P_n is a Legendre function (Abramowitz & Stegun 1965, p. 332).

Thus the effect of the spray on the external flow far from the jet is the same as that of a line sink (Taylor 1958). Since weak cross-flows do not affect the entrainment rate into jets, the same assumption is made for spray jets. With no cross-flow it is found that $E(r)/l(r)$ is proportional to the mean velocity U_j of the induced air flow in the jet. In the analysis of Ghosh & Hunt (1994) it was shown that $[E(r)/l(r)] \simeq U_j \propto r^{-1/2}$ (in spherical coordinates). Thence, since $l(r) \propto r$, from (2.4*b*),

$$v_\theta = \left(\frac{E(r)}{2\pi r\sin\theta}\right) \quad \text{as} \quad \theta \to 0 \quad \text{and} \quad r\sin\theta/l \gg 1\ . \tag{2.9}$$

From the spray solution of Ghosh & Hunt (1994)

$$E(r) = 2\pi Q_j r^{1/2}\sin\theta\ ,$$

where the parameter Q_j $\left[\text{dimension } L^{3/2}T^{-1}\right]$ that determines the strength of the air jet is defined by

$$Q_j = \frac{3}{4\beta}\left(\frac{3C_D Q_l V_0}{8a\pi}\right)^{1/2} \tag{2.10}$$

for a narrow spray, where C_D is the drag coefficient, Q_l, the liquid discharge rate, V_0 the initial droplet velocity. The Stokes' stream function in (2.7*c*) now becomes (with $n = \frac{1}{2}$)

$$\psi(r,\mu) = Q_j\tfrac{3}{2}r^{3/2}\left(1-\mu^2\right)\frac{\mathrm{d}P_{1/2}(\mu)}{\mathrm{d}\mu} = Q_j\left(-\tfrac{1}{3}r^{3/2}\left\{\mu P_{1/2}(\mu) - P_{-1/2}(\mu)\right\}\right) \tag{2.11}$$

(see Abramowitz and Stegun 1965, p. 337).

Note that $P_{1/2}(\mu)$ and $P_{-1/2}(\mu)$ are expressed in terms of elliptic integrals

$$P_{1/2}(\mu) = \frac{2}{\pi}\left[2E\left(\frac{1-\mu}{2}\right)^{1/2} - K\left(\frac{1-\mu}{2}\right)^{1/2}\right]\ , \tag{2.12}$$

$$P_{-1/2}(\mu) = \frac{2}{\pi}K\left(\frac{1-\mu}{2}\right)^{1/2}\ . \tag{2.13}$$

Thence from (2.5*a*) the full solution for the external flow around an axisymmetric spray in a weak cross-flow is given by adding the solutions derived from (2.6*b*) and (2.11) using (2.12) and (2.13), namely (in spherical polar coordinates)

$$\left.\begin{aligned} v_r &= U_0\sin\theta\cos\chi\left(1-\frac{l^2(r)}{r^2\sin^2\theta}\right) - \frac{Q_j}{2}r^{-1/2}P_{1/2}(\mu)\ , \\ v_\theta &= U_0\cos\theta\cos\chi\left(1-\frac{l^2(r)}{r^2\sin^2\theta}\right) + Q_j\frac{r^{-1/2}}{2(1-\mu^2)^{1/2}}\left\{\mu P_{1/2}(\mu) - P_{-1/2}(\mu)\right\}, \\ v_\chi &= -U_0\sin\theta\sin\chi\left(1+\frac{l^2(r)}{r^2\sin^2\theta}\right). \end{aligned}\right\} \tag{2.14}$$

https://doi.org/10.1017/S0022112098001190 Published online by Cambridge University Press

		$\theta = 0$	$\theta = \pi/2$	$\theta = \pi$
(*a*)	ψ	$\frac{4}{3}\pi r^{3/2}$	$\frac{2}{3\pi} r^{3/2} K\left(\sqrt{\frac{1}{2}}\right)$	0
	v_θ	$-\left(\frac{2}{\pi}\right) r^{-1/2} \frac{1}{\sin\theta}$	$\frac{-r^{-1/2}}{\pi} K\left(\sqrt{\frac{1}{2}}\right)$	0
	v_r	$\frac{-r^{-1/2}}{\pi}\left[2E(1) - K(1)\right]$	$\frac{-r^{-1/2}}{\pi}\left[2E\left(\sqrt{\frac{1}{2}}\right) - K\left(\sqrt{\frac{1}{2}}\right)\right]$	$-\frac{1}{2} r^{-1/2}$
(*b*)	ψ	$2r$	r	0
	v_θ	$-r^{-1} \frac{1}{\sin\theta}$	$-r^{-1}$	0
	v_r	$-r^{-1}$	$-r^{-1}$	$-r^{-1}$

TABLE 1. (*a*) Spray jet solutions, (*b*) forced jet solutions (Taylor 1958).

2.3.1. *Asymptotic limits and special cases*

The form of the external flow can be understood by calculating the velocity at particular radii using equations (2.11)–(2.14).

Near the axis of the spray

$$\text{as} \quad \theta \to 0, \quad v_r \to \frac{Q_j}{r \sin\theta} \quad \text{and} \quad v_\theta \to -\frac{2}{\pi} Q_j r^{-1/2}/(\sin\theta). \tag{2.15}$$

Note that at the edge of the jet (where $|\theta| > 0$), v_θ is finite, and the net flux into the jet per unit length is $v_\theta 2\pi r \sin\theta = -4\pi(Q_j) r^{1/2}$.

At the level of the origin of the spray jet (approximately the height of the nozzle), where $\theta = \pi/2$,

$$v_\theta = -Q_j \frac{r^{-1/2}}{2} \left\{ \frac{2}{\pi} K\left(\sqrt{\frac{1}{2}}\right) \right\} = -0.623 Q_j r^{-1/2}, \tag{2.16}$$

$$v_r = U_0 \cos\chi - Q_j \frac{r^{-1/2}}{2} \frac{2}{\pi} \left\{ 2E\left(\sqrt{\frac{1}{2}}\right) - K\left(\sqrt{\frac{1}{2}}\right) \right\} = U_0 \cos\chi - 0.13 Q_j r^{-1/2}. \tag{2.17}$$

Above this level (where $\theta > \frac{1}{2}\pi$) the sink-like effect of entrainment into the jet produces a radial flow downwards. Directly above the jet on its centreline the velocity is given by

$$\text{on} \quad \theta \to \pi, \quad \psi \to 0, \quad v_\theta \to 0, \quad v_r \to -Q_j \tfrac{1}{2} r^{-1/2}. \tag{2.18}$$

Since this analysis assumes a point source it is not an accurate description of the flow near the source of the spray at $z < Z_s$, or $r < R_j$. These analytic results were checked by comparing them with the solution that Taylor (1958) obtained for a forced air jet issuing into unbounded space from a small round orifice. The main results are compared and summarized in table 1.

In this context it is relevant to discuss some of the related issues from an earlier study by us on the induced air velocity within droplet-driven sprays (Ghosh & Hunt 1994). This study showed that the induced air flow in sprays have some of the same charactersitics as those of regular jets such as the generation of turbulence, the entrainment of air into them, and a linear growth rate of the radius. But in other ways the air flow differs because it is continually forced within the spray by the drag

https://doi.org/10.1017/S0022112098001190 Published online by Cambridge University Press

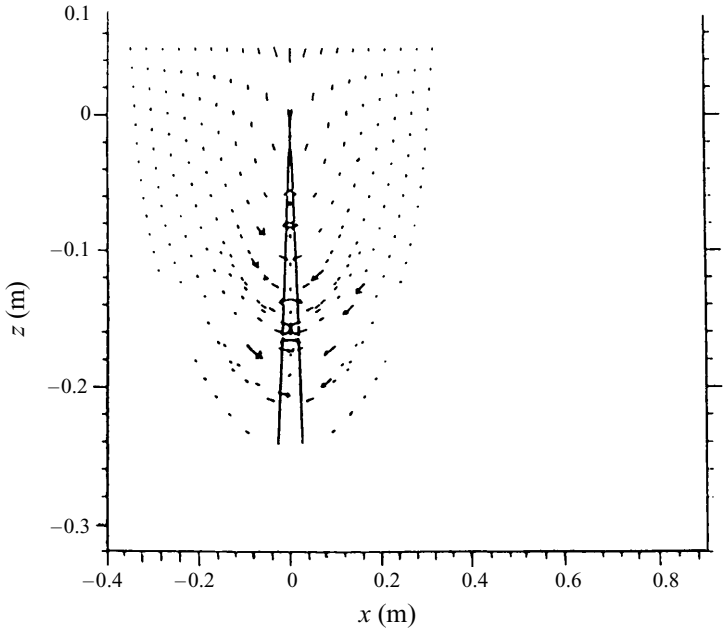


FIGURE 5. Flow vectors around zone A for the external flow without any cross-wind. The flow is driven by entrainment into the spray jet.

of the droplets, especially near the spray head and as we have just seen, this leads the average induced air velocity to decay more slowly as $r^{-1/2}$ than in a regular jet where the rate of decay is proportional to r^{-1}. Analytical results with asymptotic estimates of the induced air velocity for small and large downstream distances compared well with experimental observations as well as with estimates from a full numerical calculation at distances greater than the droplet stopping distance, $U_j \sim r^{-1}$.

From this comparison we find that v_r and v_θ in zone A for the weak cross-wind case decay more slowly as $r^{-1/2}$, rather than r^{-1} as for the forced jet. Likewise the Stokes stream function varies as $r^{3/2}$ for the spray jet solution; whereas it varies as r for the forced jet.

An alternative approach is to calculate the velocity potential for a prescribed line sink. When this is done it is found that again $v_r \sim r^{-1/2}$ as in the solutions (2.14).

In order to simplify the computation and for easier visualization, velocity vectors are plotted in figures 5 and 6 for an axisymmetric spray jet using Cartesian coordinates. Figure 5 shows how, when the cross-wind speed U_0 is zero, the velocity vectors are directed axisymmetrically in towards the spray axis. Figures 6(a) and 6(b) show how when the cross-wind speed U_0 is increased (so that $U_0 \gtrsim U_e$ at $z = 0.2$ m) the symmetry about the plane $\chi = \frac{1}{2}\pi$ is broken since the velocity vectors tend to align themselves in the direction of the cross-wind far from the jet; these are apparent in figure 6(a), where the flow is in the x-direction and the vectors are plotted in the $\chi = 0$, or (x, z)-plane where the spray jet is directed vertically downward along the z-axis. Figure 6(b) shows flow vectors in the $z = r\cos\theta$ or (x, y)-plane, where the entrainment velocity $U_e = 0.3$ m s^{-1}.

Figure 6(b) shows how the streamlines close to the spray curve in towards the centre while those starting further away first curve inwards and then follow the cross-wind. The flow stagnates at a certain distance X from the spray centreline, which

https://doi.org/10.1017/S0022112098001190 Published online by Cambridge University Press

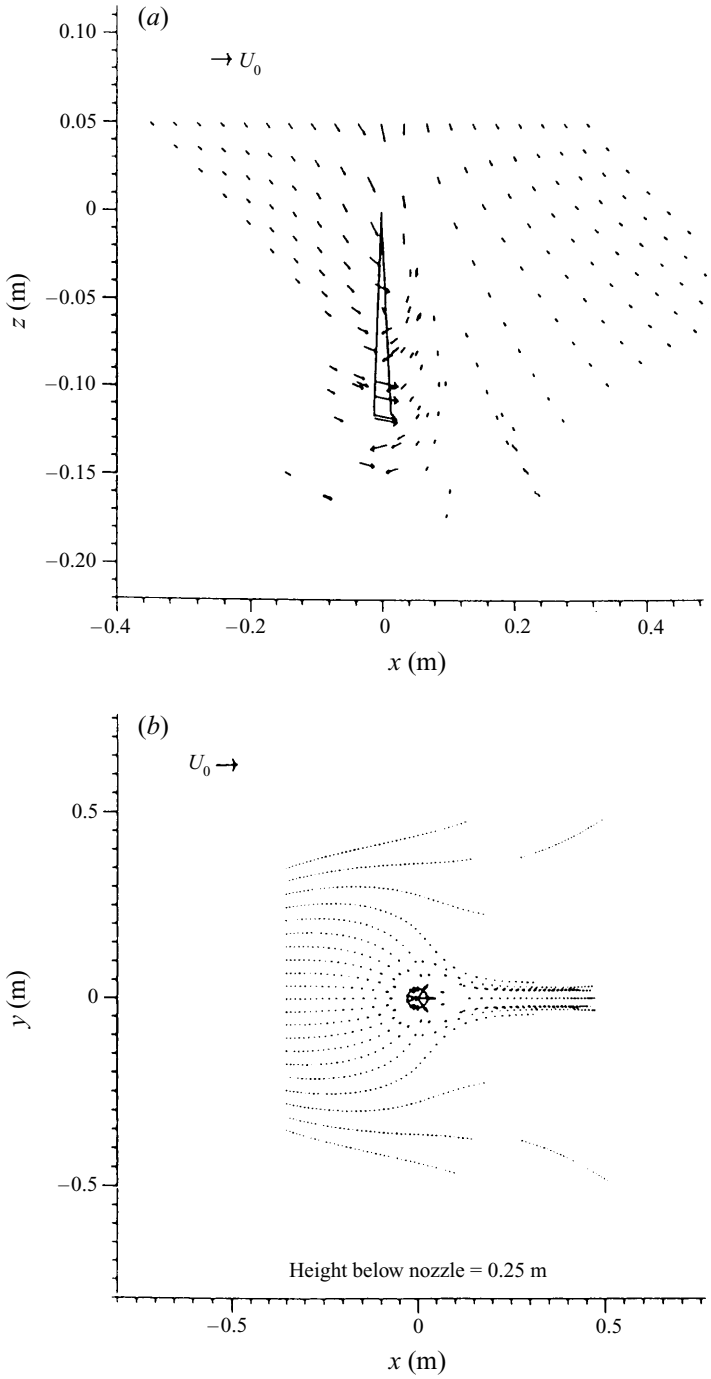


FIGURE 6. (*a*) Flow around zone A for a spray jet in a moderate cross-wind. Note the asymmetry of the flow and its alignment in the direction of the cross-wind. (*b*) A plan view of the flow vectors in a moderate cross-wind. $U_0 = 3$ m s^{-1}.

https://doi.org/10.1017/S0022112098001190 Published online by Cambridge University Press

depends on the relative magnitudes of the cross-wind speed and the centreline air jet speed (U_j/U_0). For small values of (U_j/U_0) the cross-section of the spray jet and its velocity distribution are expected to change in the same way as that of a fluid jet in a cross-flow whose inertia causes the deflection of the external flow around it and whose surface vorticity causes a pair of axial vortices on the downwind side of the spray (Coelho & Hunt 1989; Abramovich 1963). These vortices have a significant effect on the spray because they induce a back flow which reduces the tendency of the small droplets to leave the spray.

In the case of the weak relative cross-wind, there is a region below $\mathbb{B}$ below $\mathbb{A}$ (for $z > Z_{AB}$) where the air speed U_j in the spray jet is low enough that the inflow entrainment velocity U_e is less than the cross-wind speed U_0 but the air jet speed U_j in $\mathbb{B}$ is greater than the cross-wind U_0, i.e. $V > U_j > U_0 > U_e$. This means that some streamlines leave the jet removing small spray particles on the downwind side (figure 3).

By the time the spray jet has moved below region $\mathbb{B}$, although the larger spray droplets are still travelling fast enough that they are not affected by the cross-flow, the centre of the induced jet has moved a significant horizontal distance downwind ($\sim (z^2/R_j)(U_0/U_j)$) of the order of one or two diameters. In other words the spray develops a double structure consisting of the droplet region $\mathbb{C}_d$, where the flow is resisted by the larger droplets and where the streamlines diverge and are deflected downwards by their drag, and a vortical wake region $\mathbb{C}_j$ which extends downwind. The horizontal flow in $\mathbb{C}_j$ is less than U_0 until far downwind where the difference is diffused by shear stresses.

2.4. *Sprays in moderate cross-wind* ($U_j > U_0 > U_e$)

With increased cross-winds the external flow is too strong to be completely entrained downwards in the jet, i.e. $U_0 > U_e$ (e.g. for a spray $U_0 \gtrsim 5.0$ m s^{-1}). Then there is no zone $\mathbb{A}$ and the flow regime immediately below the nozzle corresponds to zone $\mathbb{B}$ (figure 3). In this case the cross-wind velocity U_0 is still generally small compared with the spray jet speed U_j. At a distance of order $z \sim R_j U_0/U_j$ (typically about 0.1 m), zone $\mathbb{B}$ changes to a double flow zone as for a weak cross-flow. This consists of $\mathbb{C}_d$, where the cross-flow experiences resistance caused by the horizontal drag force of the heavy droplets moving downwards (see § 2.3), and the zone $\mathbb{C}_j$, where the induced air jet from zone $\mathbb{B}$ is advected slightly downwind of the spray and where the momentum drag of the spray produces a wake. In the next region $\mathbb{D}$, even the droplet speeds are so reduced that the cross-wind speed is about equal to that of the droplets, i.e. $V \sim U_0$, and the heavy droplets, although still resisting the flows, are themselves advected downwind. In most agricultural sprays, by this stage the particles have impacted onto the crops.

A strong cross-wind would correspond to the case where U_0 is greater than the jet speed (i.e. $U_j \approx V$) at the nozzle and would completely blow away the jet and the spray. They could be treated as a passive source! We do not consider this case.

2.5. *Analysis of zone* $\mathbb{C}$

As explained in § 2.2, if the spray angle (c) is small, the horizontal and vertical velocity perturbations $\boldsymbol{u} = (u_x, u_y)$ can be analysed in terms of the mean horizontal and vertical force distributions denoted by $\langle F_x \rangle/\rho_a$, $\langle F_z \rangle/\rho_a$ (which are averaged over many particles but over a distance small compared to the width of the jet) on the air

https://doi.org/10.1017/S0022112098001190 Published online by Cambridge University Press

caused by the drag on the droplets:

$$U_0\frac{\partial u_x}{\partial x} = -\frac{1}{\rho_a}\frac{\partial p}{\partial x} - \langle F_x\rangle/\rho_a\ , \tag{2.19a}$$

$$U_0\frac{\partial u_y}{\partial x} = -\frac{1}{\rho_a}\frac{\partial p}{\partial y}, \tag{2.19b}$$

$$U_0\frac{\partial u_z}{\partial z} = -\frac{1}{\rho_a}\frac{\partial p}{\partial z} - \langle F_z\rangle/\rho_a \tag{2.19c}$$

and

$$\frac{\partial u_x}{\partial x} + \frac{\partial u_y}{\partial y} + \frac{\partial u_z}{\partial z} = 0. \tag{2.19d}$$

In (2.19*a*, *b*) it is assumed that the inertial terms caused by the cross-flow ($U_0\partial/\partial_x$) are large compared to those caused by the jet, i.e. $u_z\partial u_z/\partial z$ and $u_x\partial u_x/\partial x$. This is justified if

$$(U_0/U_j) \gg \ell/z = c \tag{2.20a}$$

and

$$|\,u_x\,| \ll U_0. \tag{2.20b}$$

(The distribution of the perturbed mean flow within the spray is only changed slightly by considering the small Reynolds stresses. Following Taylor (1944) we ignore these effects. However, to calculate the velocity profile in the wake downstream they have to be considered, although the net effect on the total wake deficit, $\int\int u_x \mathrm{d}x\mathrm{d}y$, is zero).

From the discussion in §2.2 the mean horizontal component per unit volume of the drag force $\langle F_x\rangle$ is related to the much larger mean vertical drag force $\langle F_z\rangle$. In the limit of a strong cross-wind when the perturbation to the cross-wind velocity U_0 is weak,

$$\langle F_x\rangle = -\frac{U_0}{V}\langle F_z\rangle, \tag{2.21}$$

where V is the droplet velocity. (Note that $\langle F_x\rangle > 0$.) $\langle F_z\rangle$ depends on the drag of individual droplets and the number of particles per unit volume (α_n) at each cross-section of the spray, and the spray width ℓ. Goldschmidt & Eskinazi (1966) have given a summary of experimental results on the widening of a plane air jet and find that the entrainment coefficient is 0.11. In addition Ghosh & Hunt (1994) have shown that the ratio of the air jet and spray jet half-width can be expressed as $\ell_a/\ell = (0.15 + c)/c$ implying that both the air jet width and the spray jet width vary linearly with z, so that for a narrow spray $\ell_a/\ell \simeq 0.15/c$ and for a wide spray $\ell_a/\ell \simeq 1$. Hence

$$\ell = cz \quad \text{for} \quad \ell > \ell_0, \quad \text{where} \quad \ell = \ell_0 \quad \text{for} \quad z = Z_0, \tag{2.22}$$

where c is the spray half-angle, Z_0 defines the value of z below which the spray is fully formed in the sense of (2.21). Note that we take as origin the geometrical origin of the distribution of the spray droplets.

Hence $\langle F_z\rangle$ is given by

$$\langle F_z\rangle = -\alpha_n \tfrac{1}{2} C_D \pi a^2 V^2, \quad \text{where} \quad \alpha_n = \alpha_{n0}(z)\mathrm{e}^{-(x^2+y^2)/\ell^2} \tag{2.23a}$$

and by continuity of the liquid flow

$$(\tfrac{4}{3}\pi a^3)\int\int V\alpha \mathrm{d}x\mathrm{d}y = Q_\ell, \tag{2.23b}$$

https://doi.org/10.1017/S0022112098001190 Published online by Cambridge University Press

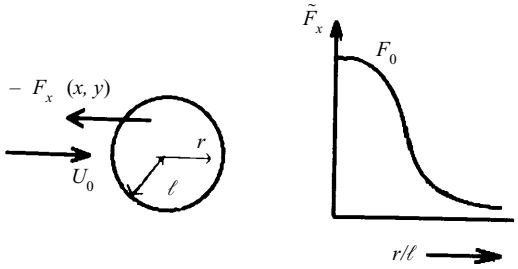


FIGURE 7. The horizontal drag force $\langle F_x\rangle(r)$ acting on the flow in the spray jet and its assumed radial profile, experienced in normalised form; $\widetilde{F_x} = \langle F_x\rangle/\rho_a$.

where Q_l is the liquid discharge rate and $\alpha = \alpha_n(\frac{4}{3}\pi a^3)$. (Note that that $0 < \alpha < 1$.) It follows from (2.23*a*) that

$$\langle F_x\rangle/\rho_a = \widetilde{F}_x = F_0 \mathrm{e}^{-(x^2+y^2)/l^2}, \tag{2.23c}$$

where

$$F_0 = \left[\frac{3C_D U_0 Q_l}{8\pi a c^2}\right]\frac{1}{z^2}\,. \tag{2.24}$$

Note that this expression is independent of V (see figure 7); the only assumption about the magnitude of V is that $V \gg U_0$. There is no need to assume that V is constant.

Solution for the horizontal perturbed motion

Taking the curl of (2.19*a*, *b*) leads to

$$U_0\frac{\partial\omega_z}{\partial x} = \frac{\partial}{\partial y}(\langle F_x\rangle/\rho_a)\,, \tag{2.25}$$

where

$$\omega_z = \frac{\partial u_y}{\partial x} - \frac{\partial u_x}{\partial y} = -\left(\frac{\partial^2\widetilde{\Psi}}{\partial x^2} + \frac{\partial^2\widetilde{\Psi}}{\partial y^2}\right) \tag{2.26}$$

is the vertical vorticity, and $\widetilde{\Psi}$ is the stream function for the horizontal flow perturbation.

Thence integrating (2.25) with the use of (2.23*b*) leads to an expression for the vertical vorticity

$$\omega_z = -\frac{2yF_0}{U_0\ell}\mathrm{e}^{-y^2/l^2}\frac{\pi^{1/2}}{2}[1+\mathrm{erf}\,(x/l)]\,. \tag{2.27}$$

From the vertical vorticity the perturbed horizontal velocity can be calculated for thin sprays in which $|\partial u_x/\partial x|$ and $|\partial u_y/\partial y|$ are much greater than $|\partial u_z/\partial z|$ so that the horizontal perturbed velocity components (u_x, u_y) can be represented by the stream function $\widetilde{\Psi}(x, y)$.

Thence from (2.26), (2.27)

$$\omega_z = -\left(\frac{\partial^2}{\partial x^2} + \frac{\partial^2}{\partial y^2}\right)\widetilde{\Psi}(x,y) = -Ay\,\mathrm{e}^{-y^2/l^2}\left[1+\mathrm{erf}\,(x/l)\right], \tag{2.28}$$

where $A = -(2F_0/U_0 l)(\frac{1}{4}\pi)^{1/4}$. Equation (2.28) is a Poisson equation satisfying the

https://doi.org/10.1017/S0022112098001190 Published online by Cambridge University Press

following boundary conditions:

$$u_y = \frac{\partial \widetilde{\Psi}}{\partial x} \to 0 \quad \text{as} \quad (x^2 + y^2) \to \pm\infty; \quad u_x = -\frac{\partial \widetilde{\Psi}}{\partial y} \to 0 \quad \text{as} \quad x \to -\infty\,. \tag{2.29}$$

Note that since the right-hand side is antisymmetric in y, $\widetilde{\Psi}$ is also antisymmetric and therefore u_x is symmetric.

The asymptotic solutions in the downstream wake are

$$\text{as} \quad x/l \to \infty, \quad \widetilde{\Psi} = -\ell^3 A \pi^{1/2} \mathrm{erf}\,(y/l)$$

so that

$$u_x = \frac{-\partial \widetilde{\Psi}}{\partial y} = -(\pi^{1/2} F_0 l/U_0) \mathrm{e}^{-y^2/l^2} \tag{2.30}$$

while upstream, as $x \to \infty$, $\widetilde{\Psi} \to 0$.

Then, since

$$\rho_a \int_{-\infty}^{\infty} u_x U_0 \mathrm{d}y = -l^2 F_0 \pi \rho_a = -\int_{\infty}^{\infty} \int_{\infty}^{\infty} \langle F_x \rangle \mathrm{d}y \mathrm{d}x\,, \tag{2.31}$$

the 'deficit' momentum flux is equal to the drag produced by the spray at each horizontal cross-section (Batchelor 1967).

We have obtained numerical solutions to (2.28) using the boundary conditions (2.29) and by prescribing values for F_0 that are suitable for typical sprays. (This is simpler than evaluating the double integrals in the closed form solution to (2.28).)

Vertical velocity perturbation

For thin spray jets, where $c \ll 1$, and a moderately strong cross-flow, so that $U_0 \gg U_j$ (i.e. the condition (2.20) is satisfied), the vertical perturbation pressure gradient in (2.19*c*) is negligible. Then the solution for u_z is given by

$$u_z = -\frac{1}{U_0} \int_{-\infty}^{x} \langle F_z \rangle / \rho_a \mathrm{d}x. \tag{2.32}$$

Thus the vertical perturbation velocity is also present in the region $\mathbb{C}_j$ downwind of the region $\mathbb{C}_j$ containing the large droplets and where $\langle F_z \rangle \neq 0$.

Given the distribution of α and thence the derivation of $\langle F_z \rangle$ from (2.23*a*), it follows that the profile of u_z has the simple form

$$u_z = +\frac{V F_0 l}{U_0^2} \mathrm{e}^{-y^2/l^2} \pi^{1/2} (1 + \mathrm{erf}\,(x/l)). \tag{2.33}$$

2.6. *Characteristics of the flow zones*

It is instructive to compare the magnitudes of the centreline vertical jet velocities $U_j = u_z(x = y = 0)$ in the different regions of the spray jet. From (2.21), (2.24) and (2.33), it follows that

$$\text{in} \quad \mathbb{C}_d, \quad U_j \sim \frac{V}{U_0} \frac{Q_l}{az} \frac{3C_D}{8\pi c}, \tag{2.34a}$$

whereas, from equation (24) of Ghosh & Hunt (1994),

$$\text{in} \quad \mathbb{A}, \quad U_j \sim \left[\frac{V Q_l}{az}\right]^{1/2} \left(\frac{3C_D}{8\pi}\right)^{1/2} \frac{3}{4\beta}\,. \tag{2.34b}$$

https://doi.org/10.1017/S0022112098001190 Published online by Cambridge University Press

Note how U_j decreases more rapidly with z in $\mathbb{C}$, in proportion to z^{-1}, than in region $\mathbb{A}$, where U_j decreases in proportion to $z^{-1/2}$.

Note that Q_l may be estimated in terms of parameters at $z = Z_s$ where the spray jet is formed as $Q_l \simeq 2\pi\alpha_j R_j a V_j$, assuming $Z_s \simeq Z_0$ and $l_0 \simeq R_j$. (If a liquid stream of radius R_j breaks up into a spray at $z = Z_s$ then $\alpha_j \simeq 1$. But for most sprays $\alpha_j \ll 1$.) At the level Z_{AB} where region $\mathbb{A}$ joins region $\mathbb{B}$, and by definition the cross-stream velocity is of the order of the entrainment velocity, it follows from (2.34*b*) that $U_0 \sim U_e \sim \beta U_j$, and thence the distance to Z_{AB} is given by

$$Z_{AB} \sim [V Q_l / a]^2 / U_0^2. \tag{2.35a}$$

Using the above estimate for Q_l leads to

$$| Z_s - Z_{AB} | / R_j \sim (V/U_0)^2 \alpha_j. \tag{2.35b}$$

From (2.20) it follows that the approximations of region $\mathbb{C}$ apply where $U_0/U_j > c$. Thence from (2.34*a*) the distance to the border between regions $\mathbb{B}$ and $\mathbb{C}$ is given by

$$| Z_s - Z_{BC} | / R \sim \alpha_j (V/U_0)^2. \tag{2.35c}$$

The equivalence of the order of magnitude estimates (2.35*b*, *c*) shows that the distance to the matching region $\mathbb{B}$ is of the order of $R_j \alpha_j (V/U_0)^2$.

Across this matching zone $\mathbb{B}$ the differences between solutions given in § 2.4 for $\mathbb{A}$ and in § 2.5 for $\mathbb{C}$ show that there is a change in the magnitude of u_x. At the bottom of zone $\mathbb{A}$ where $z \sim Z_{AB}$, and $(x^2 + y^2)^{1/2} \lesssim l$,

$$u_x \sim -U_e \left(\sim \beta u_j^{(A)} \right) \sim U_0, \tag{2.36a}$$

where $x \gtrsim l$, $u_x \ll U_0$.

While at the top of zone $\mathbb{C}$, from (2.30) and (2.35*b*), at $z \sim Z_{BC}$, and $(x^2 + y^2)^{1/2} < l$,

$$u_x \sim \frac{-l(z = Z_{BC}) F_0}{U_0} \sim -U_0 \left(\frac{U_0}{cV} \right) \sim -U_0 \left(\frac{U_j}{V} \right), \quad \text{since} \quad \frac{U_0}{U_j} \sim c. \tag{2.36b}$$

Note that downstream, where $x > l$ and $|y| \lesssim l$, u_x remains of the same order as given by (2.36*b*). Since in $\mathbb{C}$, U_j is always less than V, u_x in $\mathbb{C}$ is less than the horizontal perturbation velocity at the bottom of zone $\mathbb{A}$, which is consistent with zone $\mathbb{C}$ having less effect on the oncoming flow.

The streamlines in region $\mathbb{C}$ for an axisymmetric spray are plotted in figure 8(*a*) where $U_0/U_j \simeq 0.15$ ($U_0 \simeq 3$ m s^{-1}) which shows how the resistance to the incoming cross-flow caused by the spray droplet forces the streamlines of the initially uniform cross-flow to diverge outwards and eventually again become parallel at large downwind distances. When the cross-wind speed is increased (figure 8*b*) so that $U_0 \gtrsim \frac{1}{2} U_j$ (or 9.0 m s^{-1} in a typical spray jet), the external flow is not significantly perturbed and the streamlines are almost parallel.

In this analysis of zone $\mathbb{C}$ the effect of the spray on the cross-wind is modelled as a porous resistive cylinder. However, below this region (a distance of the order $a(\rho_l/\rho_a)\ln(V/U_j) \simeq 1$ m for a spray jet) the droplet speed V is sufficiently reduced by drag so that $V \sim U_0$ and the cross-wind advects the heavy droplets. This stage is a new flow zone $\mathbb{D}$ where the entire spray begins to be advected downwind. (In many geophysical problems this is the region of greatest interest.) A computer model has been developed based on the analysis of zones $\mathbb{A}$ and $\mathbb{C}$, for calculating and plotting spray droplet trajectories as a function of the cross-wind speed, the liquid discharge rate, spray angle, etc. This is described in the following section.

https://doi.org/10.1017/S0022112098001190 Published online by Cambridge University Press

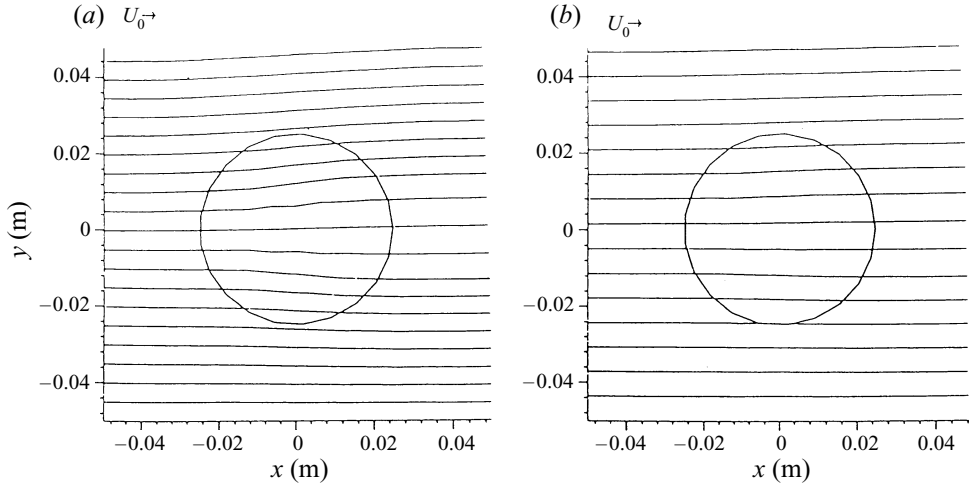


FIGURE 8. (*a*) Flow in zone ℂ for a moderate cross-wind speed (3 m s^{-1}) where $U_0/U_j \simeq 0.15$. Here the spray jet acts on the flow as if it was a porous resistive body. Notice that the streamlines of the approach flow diverge and eventually become parallel. (*b*) Weakly perturbed flow in zone ℂ in a strong cross-wind (9 m s^{-1}) when $U_0 \geqslant 0.5U_j$. Drop velocity = 20 m s^{-1}, $Q_l = 7 \times 10^{-5}$ m^3 s^{-1}), spray angle = 0.1°, drop radius = 100 μm, height below nozzle = 0.25 m.

3. Spray droplet trajectories in a cross-flow

3.1. *Axisymmetric spray*

In the preceding discussions we presented models to predict external air flow around the spray jets and also the induced air flows within sprays covering cases where the cross-flow did and did not have an effect. These flows are necessary for the prediction of the relative velocity of the droplets and thence the droplet trajectories.

Previous work concerned with predicting spray droplet movement has tended to focus on two distinct situations: (i) droplet movement close to the nozzle where considerations of air drag have been assumed to determine air entrainment, and (ii) 'droplet' movement further downwind where the droplets move under their own weight and fluctuating drag forces caused by the turbulent cross-wind. The latter situation which is more relevant to estimating the deposition of droplets onto plant surfaces has been studied more extensively than the former. For instance Bache & Sayer (1975) and Dumbauld, Rafferty & Bjorkland (1977) derived expressions for the deposit distribution downwind of a line spray source. Also, random walk models have been used to predict the trajectories of droplets in turbulent air flows (e.g. Thomson & Ley 1983; Picot, Kirstmanson & Basak-Brown 1986; Legg & Raupach 1982). In contrast the only reported work which partially deals with the former aspect is by Miller & Hadfield (1989) who used the more restrictive model of Briffa & Dombrowski (1966) to estimate the overall entrained air velocities.

In the present study we have been more concerned with near-field droplet movement and we describe models which predict spray droplet trajectories by first accurately determining entrained air characteristics without any empirical input.

The following assumptions are made:

(i) all the droplets are spherical;

(ii) no interaction occurs between droplets – which implies the exclusion of processes like secondary breakup and coalescence.

With the above assumptions, the equations of motion for droplets in the axial and

https://doi.org/10.1017/S0022112098001190 Published online by Cambridge University Press

radial direction reduce to

$$\frac{\mathrm{d}V_z}{\mathrm{d}t} = -\frac{3}{8}\frac{C_D}{a}\frac{\rho_a}{\rho_l}V_R(V_z - u_z) + g, \tag{3.1}$$

$$\frac{\mathrm{d}V_r}{\mathrm{d}t} = -\frac{3}{8}\frac{C_D}{a}\frac{\rho_a}{\rho_l}V_R(V_r - u_r), \tag{3.2}$$

where g is the gravitational acceleration. In (3.1) and (3.2) the symbols V and u denote the liquid and air velocities respectively and the other terms have their usual meanings. In general the equation of motion of a droplet is more complicated than (3.1) and (3.2). Among the forces neglected in these equations are the lift forces due to droplet rotation and shear, the force due to virtual mass and the Basset force (see Hunt *et al.* 1994).

In (3.1) and (3.2)

$$V_R = \left[(V_z - u_z)^2 + (V_r - u_r)^2\right]^{1/2}. \tag{3.3}$$

In general the fluid velocity u_z, u_r should include both the mean and turbulent components. However, in these simulations of realistic droplets moving across the near field of a jet the effects of turbulence do not significantly affect the trajectories as confirmed by a detailed study of a comparable jet problem (Perkins, Ghosh & Phillips 1991).

Zone A

The cross-sectional averaged axial induced mean air velocity, u_z, was used in (3.3), based on the results of the one-dimensional model (Ghosh *et al.* 1991), in which

$$u_z = \frac{3}{4\beta}(\lambda_1)^{1/2}z^{-1/2} \quad \text{for} \quad r < l(z)\,, \tag{3.4}$$

where β is the entrainment coefficient (~ 0.1) and

$$\lambda_1 = \frac{3C_D Q_l V_j}{8a\pi}\,, \tag{3.5}$$

where Q_l is the liquid discharge rate from the spray and V_j the initial droplet velocity.

The radial induced air velocity u_r was obtained by a numerical two-dimensional model (Ghosh & Hunt 1994) based on the Reynolds average equations of motion with forcing for steady axisymmetric flow. Recast into a similarity form the governing differential equation for u_z in the axisymmetric two-dimensional model is

$$\frac{\mathrm{d}^2 f}{\mathrm{d}\eta^2} + \frac{1}{\eta}\frac{\mathrm{d}f}{\mathrm{d}\eta} + \frac{A}{2}f^2 + Aff'\eta + Bh(\eta) = 0, \tag{3.6}$$

where $\eta = r/l$, and $f(\eta) = u_z/u_{z,0}$, where $u_{z,0}$ is the centreline air velocity. Also $A = c/\lambda_v$ where λ_v is a constant of proportionality used to parameterize the eddy viscosity of the turbulent air jet, $B = (16\beta^2/ac^2)A$, $\lambda_2 = (3C_D/8a)(\rho_a/\rho_l)$, and $h(\eta)$ is a function that prescribes the radial distribution of the large droplets.

Assuming that each droplet behaves as a rigid sphere, the drag coefficient C_D is taken as (Wallis 1969)

$$\begin{aligned} C_D &= \frac{24}{|Re|}\left(1 + 0.15|Re|^{0.687}\right) \quad \text{for} \quad |Re| \leqslant 1000 \\ &= 0.44 \qquad\qquad\qquad\qquad\quad \text{for} \quad |Re| > 1000, \end{aligned} \tag{3.7}$$

where Re is the droplet Reynolds number which depends on the magnitude of the

https://doi.org/10.1017/S0022112098001190 Published online by Cambridge University Press

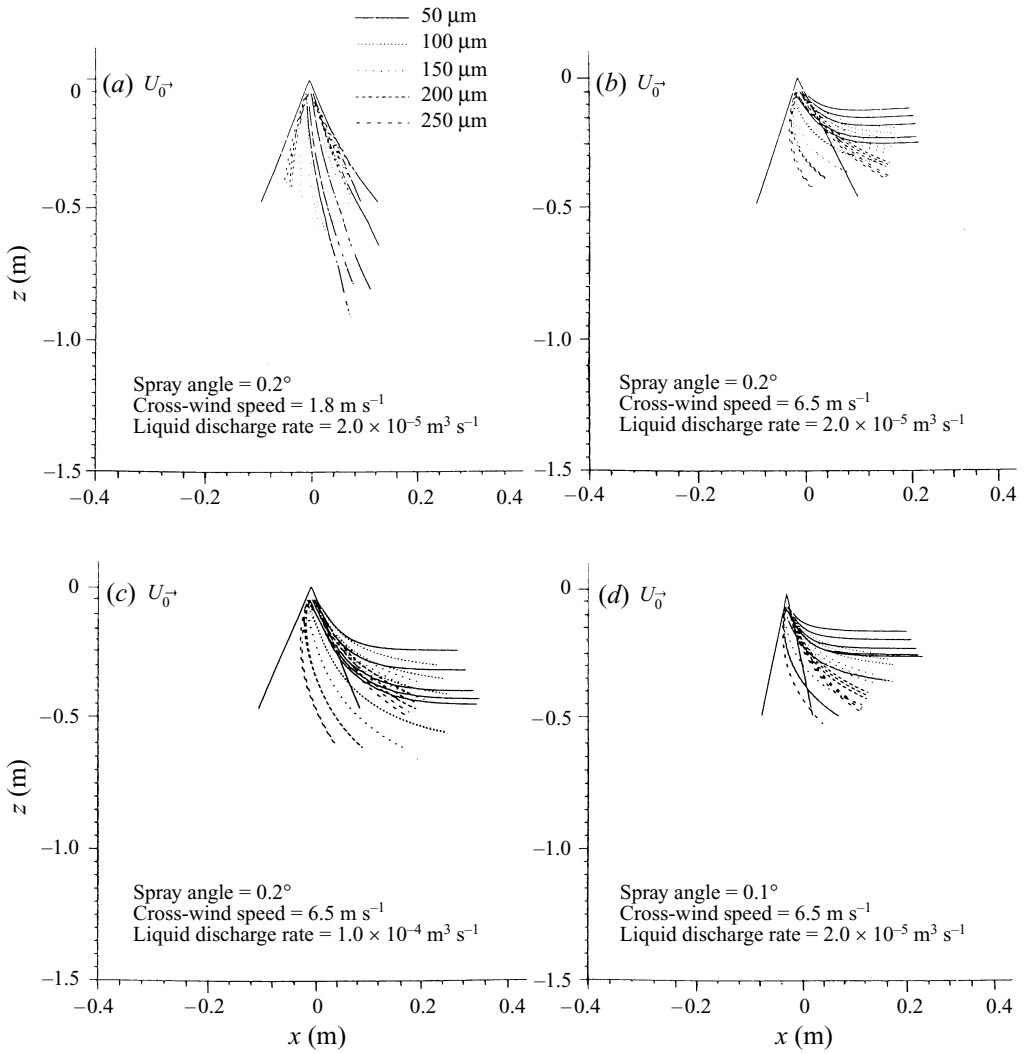


FIGURE 9. Droplet trajectories for an axisymmetric spray. (*a*) Weak cross-wind; note that small droplets tend to aggregate towards the spray centreline. (*b*) Strong cross-wind; note the immediate detrainment of the 50 μm droplets. (*c*) Effect of a high liquid discharge rate (resulting in a high induced air speed U_j) on spray droplet trajectories. Note that this reduces spray detrainment particularly in zone A. (*d*) The effect of spray angle on droplet detrainment. Note that detrainment is enhanced with narrower angles.

relative velocity between the gas and the droplet phase:

$$Re = 2(V - u)\, a/v \ . \tag{3.8}$$

The trajectories of the small droplets were obtained by integrating (3.1) and (3.2) using (3.3), (3.4), (3.7), (3.8), the integration of (3.6) and the formulae (2.14) of § 2.3 for zone A.

Figure 9 shows some simulated droplet trajectories for five different sizes for the case of a weak cross-wind ($U_0 \sim 2.0$ m s^{-1}). From this figure we find that up to about 0.1 m below the nozzle the spray droplets are hardly affected by the cross-wind. The 50 μm droplets tend to aggregate along the spray centreline – this is only to be

https://doi.org/10.1017/S0022112098001190 Published online by Cambridge University Press

expected because these small droplets tend to follow the converging streamlines of the air flow. From the same figure we also note that, at this distance below the nozzle, the larger spray droplets deviate little from the nominal spray cone angle. An order of magnitude estimate using the one-dimensional model shows that the characteristic centreline air velocity U_j at $z = 0.1$ m for this droplet size is of the order of 12.0 m s^{-1}, which is six times higher than the cross-flow.

Here, it is worth pointing out that previous work on liquid sprays assumed that the velocity field of the gas is similar to that of a free circular jet (Lee & Tankin 1984). However, our theoretical and experimental analyses (Ghosh *et al.* 1991) showed that this assumption is incorrect, both as regards the mean flow and the structure of turbulence because the air jets in droplet-driven sprays are characterized by much smaller scales of turbulence than the eddy structure of regular jets. As a result the most realistic way of modelling droplet trajectories in sprays is perhaps the scheme outlined in the analysis.

For an axisymmetric spray (without a cross-wind) Lee & Tankin (1984) observed the streamline convergence on the centreline in their experiments and in their simulation, but did not provide any physical explanation for this effect.

Zone ℂ *for a moderate cross-wind*

The situation is drastically changed when there is a moderate cross-wind, i.e. $U_0 \geqslant U_e$ (or $U_0 = 6.5$ m s^{-1} for a spray). See figure 9(*b*). Now the small spray droplets are immediately detrained from the spray by the cross-wind and the results of § 2.4 for zone ℂ can be used. In fact, the whole spray bends in the direction of the cross-wind and, as expected, the extent of deflection at a given downwind distance becomes less pronounced for increased spray droplet sizes.

The fact that the ratio of the cross-wind speed to the air jet speed is a crucial determining factor in the quantification of spray drift is well illustrated by comparing figures 9(*b*) and 9(*c*). In both these cases the cross-wind speed is kept fixed at 6.5 m s^{-1}. In figure 9(*c*) the liquid discharge rate Q_l is increased from 2.0×10^{-5} m^3 s^{-1} to 1.0×10^{-4} m^3 s^{-1} and as a result the induced air velocity U_j is increased by a factor of 2.24 (equation (3.4)). The effect of this increase is most apparent in the droplet trajectories particularly of the smaller ones where we observe that the extent of spray detrainment is significantly lowered. The effect of the spray angle on spray droplet detrainment is demonstrated in figures 9(*b*) and 9(*d*). We find that spray droplets are more prone to detrainment for narrow sprays.

In all the simulations shown (figures 9(*a–d*) the cross-wind was uniform. We also investigated the effect of a linear profile in the upwind $U_0(z)$ which increased linearly with height from the ground (fixed at 0.5 m below the nozzle) until it attained a value of 6.5 m s^{-1} at the nozzle. This is shown in figure 10. When we compare with figure 9(*b*) which corresponds to the case of a uniform velocity profile, we observe very little effect on the spray droplet detrainment. As explained the droplet detrainment is slightly reduced with a linear velocity profile, for the same value of U_0 at the height of the spray.

3.2. *Non-axisymmetric sprays with weak cross-wind*

The most convenient way to model a non-axisymmetric spray jet (such as agricultural flat-fan sprays which are usually wide-angled and thin) is by assuming that the droplets issue radially from the nozzle at an angle $\theta_j(\chi)$ where $\chi = \tan^{-1} x/y$, which is the angular displacement in the horizontal plane. For reasons given by Ghosh & Hunt (1994) the cross-sectional shape of the air jet is determined by the radial flow

https://doi.org/10.1017/S0022112098001190 Published online by Cambridge University Press

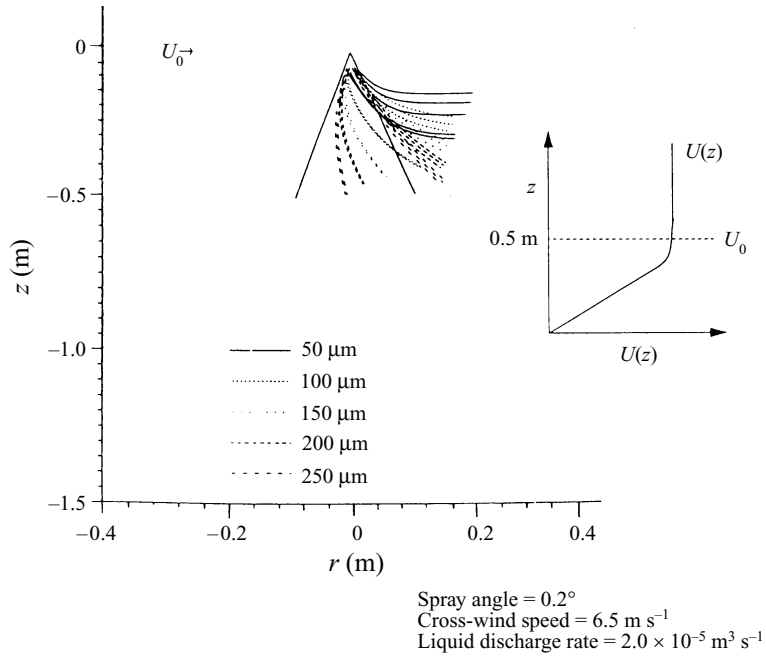


FIGURE 10. Effect of a linear velocity profile on spray droplet detrainment. Note that droplet detrainment is slightly reduced with a linear profile.

of spray droplets, or by entrainment depending on whether $\theta_j(\chi)$ is greater or less than about β ($\simeq 0.1$, the angle of an entraining jet). For the wide 'faces' of a flat-fan spray, i.e. for $|1/\pi - (l_a/z)| > \chi > (l_a/z)$, the angle is determined by entrainment, i.e. $\theta \lesssim \beta$; while for the side edges, where $|\chi| < l_a/z$, the wide angle is $\theta \simeq l_a/\lambda z$, where λ is determined by the initial spray angle and not significantly by the dynamics. See figure 11.

As before, a one-dimensional analysis is invoked, which includes the entrainment law, the void fraction, the drag on the droplet, the rate of change of average momentum of the droplet and the rate of change of momentum flux of the air jet (see equations (41)–(45), Ghosh & Hunt 1994). It is found that the axial induced air velocity is:

$$U_j = \left(\frac{9C_D Q_l V_j}{32a\pi\beta}\right)^{1/2} z^{-1/2} \tag{3.9}$$

and the air jet width

$$l_a = (2/3)\,\beta z. \tag{3.10}$$

From (3.9) we obtain the centreline variation of the air velocity. Since experimental observations show that in the y-direction across the centreline the velocity profile $u_z(y)$ is approximately Gaussian, we have

$$u_z = U_j(z)\exp\left(-\lambda^2 y^2/l_a^2(z)\right), \tag{3.11}$$

where l_a/λ is the approximate spray width (given by experiment) and U_j is given by (3.9).

The mean horizontal velocity u_x in the jet can be derived from the continuity

https://doi.org/10.1017/S0022112098001190 Published online by Cambridge University Press

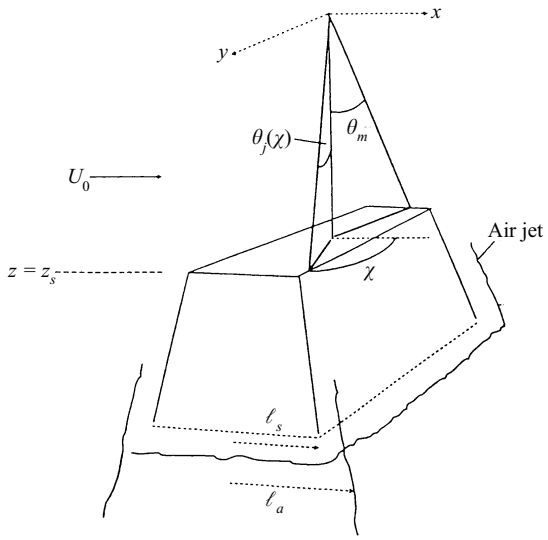


FIGURE 11. Schematic of a non-axisymmetric flat-fan spray showing the cross-section for m$\theta_j(\chi)$ of the spray jet at $z = z_s$ and the narrowest width of the air jet ℓ_a and the spray (ℓ_s). In the other direction the spray and jet angles are the same θ_m.

equation (2.19*d*). One obtains after simplification

$$u_x \simeq -\frac{4}{9_\lambda}\beta U_j(\pi^{1/2})\mathrm{erf}\left(\frac{3\lambda x}{2\beta z}\right) + \frac{x}{3z}U_j\ . \tag{3.12}$$

In this category of weak cross-winds ($U_0 \ll U_e$), a similar solution can be constructed to that in § 2.3. In zone 𝔸 streamlines enter the spray, and below zone 𝔸 where $U_0 > U_e$ some streamlines leave zone 𝔸 and carry the spray droplets downwind.

Non-axisymmetric spray in moderate cross-wind

In the presence of a moderate cross-flow U_0 so that $U_0 \gg U_e$, and $U_0/U_j \gg c$ (cross-flow perpendicular to the large angle plane), the air flow passes through the spray jet, but the bulk of the droplets offer resistance to the cross-flow and the air flow is deflected. If the shape of the spray defined by $\theta_j(\chi)$ is so non-axisymmetric as to be flat in the direction perpendicular to the wind, so that $\frac{1}{2}[\theta_j(\chi = 0) + \theta_j(\chi = \pi)] \gg \frac{1}{2}[\theta_j(\chi = \frac{1}{2}\pi) + \theta_j(\chi = \frac{2}{3}\pi)]$, the resistance of the spray leads to two vortex sheets being shed from the edges of the spray. If the boundaries of the spray are defined by $|y| = z\tan\theta_m$ (for our calculations we have chosen $\theta_m = 0.3\pi$), where θ_m is the maximum value of θ_j at $\chi = 0, \pi$, then with the usual notation we have

$$U_0\frac{\partial}{\partial x}\left(\frac{\partial u_x}{\partial y} - \frac{\partial u_y}{\partial x}\right) = -F_0\delta(x)[1 - H(|y| - z\tan\theta)] \tag{3.13}$$

(where $H(|y| - z\tan\theta)$ is the Heavyside step function) or

$$U_0\frac{\partial \omega_z}{\partial x} = -F_0\delta(x)[1 - H(|y| - z\tan\theta)] \tag{3.14}$$

which implies

$$\omega_z = \frac{-F_0}{U_0}H(x)[1 - H(|y| - z\tan\theta)] \tag{3.15}$$

https://doi.org/10.1017/S0022112098001190 Published online by Cambridge University Press

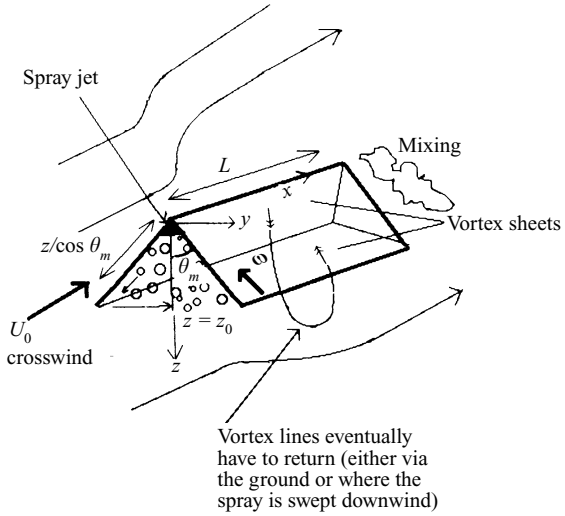


FIGURE 12. Schematic of the flow pattern when an external cross-wind impinges on a flat-fan spray, with maximum semi-angle θ_m, and forming 'vortex sheets' at the edges of the spray jet. Here the vectors $\twoheadrightarrow$ denote vorticity.

and

$$\omega_y = \frac{F_0}{U_0} \tan\theta H(x)[1 - H(|y| - z\tan\theta)], \tag{3.16}$$

where

$$F_0 = \frac{3C_D Q_l U_0}{16a\pi z^2 C}.$$

From (3.15)–(3.16) we find that two vortex sheets are created. Inside the vortex sheet there is a velocity defect with $u_x \sim -F_0/U_0$; $u_y = 0, u_z = 0$. Also because of this deficit the flow is deflected around the wake.

This induced velocity can be calculated by Biot-Savart law, by using the solution for two semi-infinite vortex sheets extending downwards a distance $z = Z_{CD}$ which is then at the bottom of region $\mathbb{C}_D$. Note that the vortex lines eventually will have to return either via the ground or in the flow below the region $\mathbb{C}_D$ of the spray jet, say $z \leqslant 3Z_{CD}$, and where the spray is swept downwind, i.e. $x \simeq Z_{CD}$ (see figure 12 of this paper and also Smith & Mungal (1998) for a further discussion of the structure of cross-flow jets).

From the Appendix the velocity perturbations in spray coordinates can be obtained by adding the vortex sheet solutions from (A.6) and (A.7). This gives

$$u_x(x,z) = -\frac{2\gamma}{4\pi}\left(\tan^{-1}\frac{x}{\tan\theta_m(x^2+z^2)^{1/2}} + \tan^{-1}\frac{x}{z\sin\theta_m} + \pi - \theta_m\right). \tag{3.17}$$

And likewise, the vertical upward velocity along the centreline is given by

$$\text{for } |y| \ll Y\,; z < Z, u_z(z) = \frac{\gamma\sin\theta_m}{4\pi}\left(\ln\left|\frac{(x^2+z^2)^{1/2} - z\cos\theta_m}{(x^2+z^2)^{1/2} + z\cos\theta_m}\right| - \ln\left|\frac{Y^2}{x^2+z^2\sin^2\theta_m}\right|\right). \tag{3.18}$$

Note that evaluating u_z requires specifying the lateral extent of the vortex lines Y; we assume $Y \simeq 3Z_{CD}\tan(\theta_m)$. The appropriate length scale that can be formed for an

https://doi.org/10.1017/S0022112098001190 Published online by Cambridge University Press

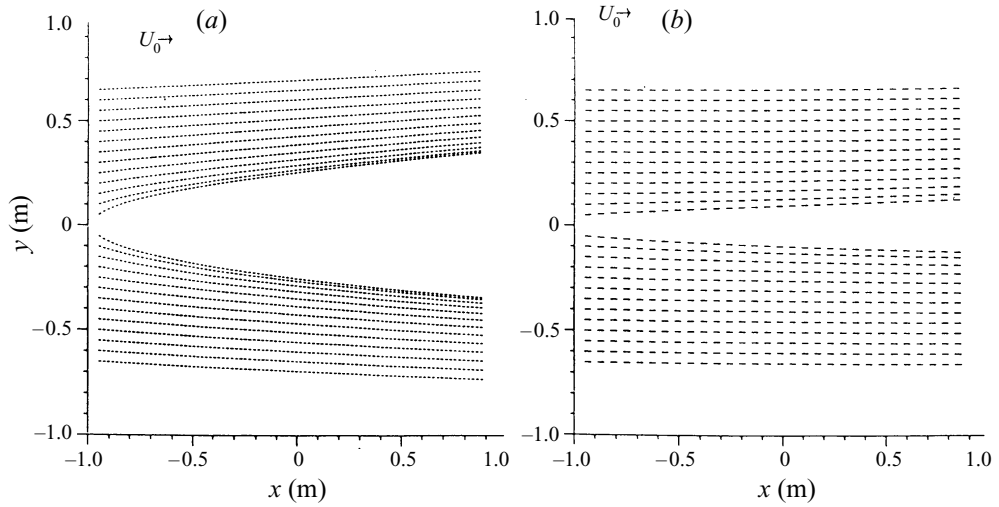


FIGURE 13. Streamlines for an external flow impinging onto a flat-fan spray. (*a*) Weak uniform cross-flow 1 m s^{-1}; note how the flow diverges . (*b*) Strong uniform cross-wind 3 m s^{-1}. $U_j = 10$ m s^{-1}.

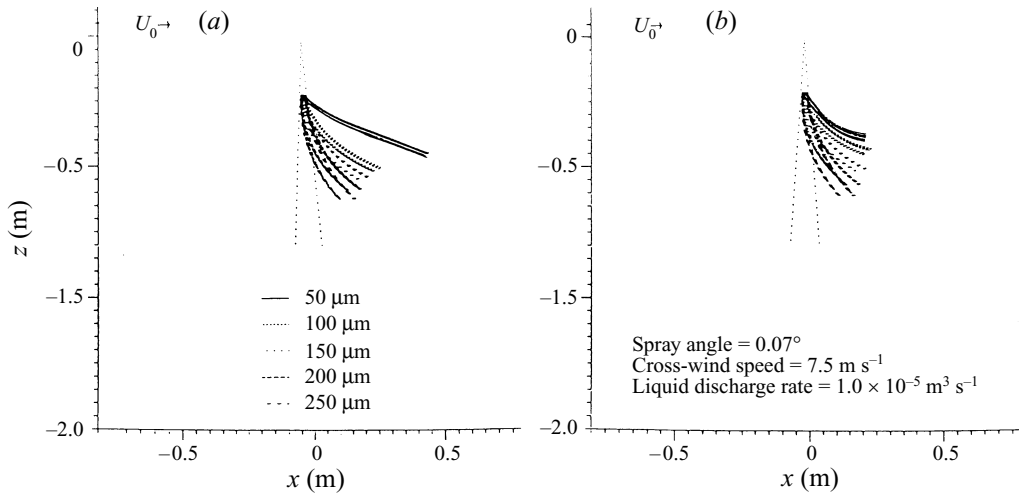


FIGURE 14. (*a*) Flat-fan spray droplet trajectories. (*b*) Flat-fan spray droplet trajectories without the effect of air velocity perturbations. Comparison with (*a*) shows that velocity perturbations enhance the dispersion of small droplets.

order of magnitude estimate of Y in terms of the jet momentum and the cross-wind speed is $[(F_0/\rho_j)1/U_0^2]^{1/2}$. For typical spray parameters and for a moderate cross-wind speed of 3.0 m s^{-1}, $Y \sim 1$ m.

Figures 13(*a*) and 13(*b*) show the effect of the air velocity perturbations on the external flow in the (x, y)-plane only for a weak and strong cross-flow respectively.

Having obtained expressions for the mean induced air velocity components and the velocity perturbations in the x-, y-, z-directions the spray droplet trajectories are obtained by integrating the Euler equations (3.1) and (3.2). These are shown in figures 14(*a*) and 14(*b*) where the droplet trajectories for a flat-fan spray are plotted in the (x, z)-plane. It is observed that the vortex sheet wake velocity perturbation

https://doi.org/10.1017/S0022112098001190 Published online by Cambridge University Press

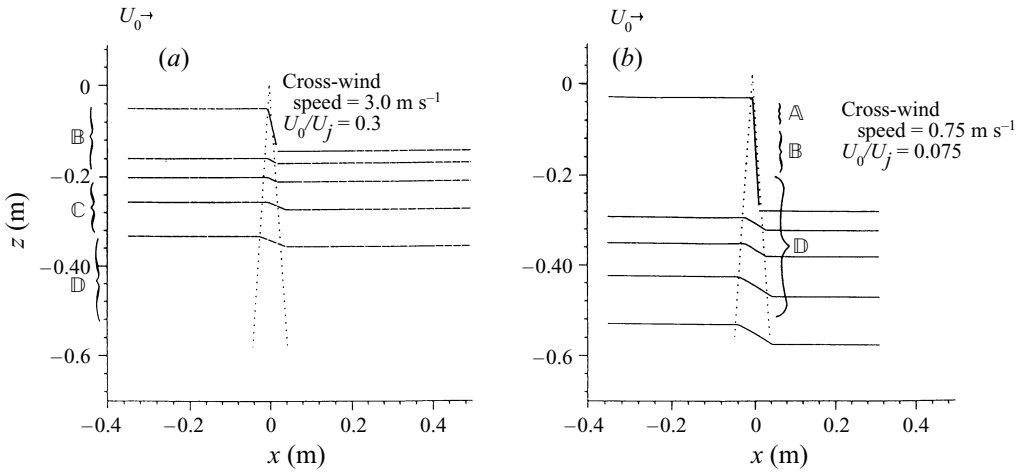


FIGURE 15. Numerical simulation of Phillips *et al.*'s flow visualisation experiments. (*a*) Moderate cross-wind; note that near the nozzle the external air is sucked in downwards along the spray centreline, whereas at large distances below the nozzle the external air flow is only slightly deflected. (*b*) Weak cross-wind. Spray angle = 0.07°, liquid discharge rate = 1.0×10^{-5} m^3 s^{-1}

has significant effects on the 50–100 μm droplets. Without the perturbations even the 50 μm droplets trajectories segregate into distinct size classes, which is not likely to happen. In general it is also observed that the effect of the air velocity perturbation diminishes with larger droplets.

3.3. *Comparison of model computations with flow visualization experiments*

Finally, we have made qualitative comparisons of the interaction of a cross-flow and a flat-fan spray with recent flow visualization experiments of Phillips, Miller & Thomas (1998) who investigated the interaction between an approximately uniform wind tunnel cross-flow and an agricultural flat-fan spray (liquid discharge rate of 1.0×10^{-5} m^3 s^{-1}), placed 0.5 m above the flow. From their streak photographs the pattern of the mean streamlines can be estimated.

The model developed here was applied to calculating the air flow around and into their flat-fan jet (see figures 15(*a*) and 15(*b*)). For their flat-fan spray we estimate the induced air jet velocity $U_j \sim 10$ m s^{-1} in the vicinity of the nozzle (see Ghosh & Hunt 1994). Likewise the entrainment velocity $U_e \sim 1$ m s^{-1}. In our terminology the Phillips *et al.* (1998) cross-wind speed $U_0 \sim 3$ m s^{-1} is 'moderate'. For this case $U_0 > U_e$, and since U_j decreases with increasing distance (z) below the nozzle, $U_j \sim U_0$ at $z \sim 0.2$ m s^{-1}.

Phillips *et al.* (1998) (figures 6*a* and 6*b*) ($0.1 < z < 0.2$) used tracer bubble trajectories to estimate air flow streamlines. It was found that near the spray ($z < 0.1$ m) the streamlines were entrained downward into the jet. However for $z > 0.2$ m, they show only slight vertical deviation. In general the extent of deviation decreases with increasing distances below the nozzle. Beyond distances $z > 0.3$ m (zone 𝔻) the cross-flow penetrates the spray with marginal deviation, but the spray droplets themselves are deflected. The changes in the streamline pattern were also seen in the model computations (figure 15*a*). Figure 15(*b*) shows the corresponding computations to compare with Phillips *et al.* (1998) for the low cross-wind case. We find that at distances up to 0.2 m (regions 𝔸 and 𝔹) below the nozzle, the cross-flow is drawn towards the spray centreline; on entering the main body of the spray the surround-

https://doi.org/10.1017/S0022112098001190 Published online by Cambridge University Press

ing air is rapidly accelerated downwards and inwards towards the centreline. This is because the entrainment velocity $U_e > U_0$. Beyond $z \geqslant 0.3$ m, the cross-wind is able to penetrate the spray. This would correspond to the flow zone ℂ (figure 3*b*). Comparing our calculations with the experiment for this case, we observe that indeed up to 0.2 m below the nozzle the cross-flow is drawn towards the centreline both in the model and the flow visualization studies. However, for large distances below the nozzle ($z > 0.3$ m), the model shows a stronger spray penetration than is observed. Although at this stage of our research we are unable to present further quantitative verifications, the broad agreement between the flow visualization experiments and the numerical simulation of the flow supports our theoretical model for the dominant mechanisms that operate on different zones of a spray when it is subjected to an external cross-wind.

4. Conclusions

In this paper we have investigated some basic aspects of the dynamics of spray jets in a cross-flow. It has been shown that quite different patterns of air flow and droplet dispersion occur at different distances from the nozzle depending on the ratio of the air speed in the induced air jet to the relative cross-wind speed or the tractor speed. For example we find that for the case of a weak cross-wind, in the region immediately below the nozzle, the spray centreline acts as a line sink for the external flow. When the cross-wind is relatively strong the spray droplets can act as a porous resistive body over a certain distance below the nozzle, which deflects the flow lines. Analytical and numerical models are presented, along with plots of spray droplet trajectories for five different size classes as a function of the cross-wind speed and other spray parameters like the spray angle, the liquid discharge rate and droplet density. No special empirical factors are introduced into the models, though conventional assumptions were made about certain local flow mechanisms. For practical purposes it might be useful to develop formulae to describe the flow between these regimes. The predictions are consistent with the preliminary qualitative measurements of the droplet pattern and of the air movement over the sprays.

The analysis should be extended for application to other geophysical problems where local streams of particles and bubbles drive flows at angles to large-scale cross-flows, such as clouds, volcanoes, bubble plumes etc.

This research was funded by the Agricultural and Food Research Council and was expertly monitored by Dr Paul Miller at the Silsoe Research Institute. We are grateful for many valuable comments and insights from him and our colleagues at Cambridge, especially Jeremy Phillips.

Appendix

The purpose of this appendix is to calculate the velocity field produced by a strip of a vortex sheet. (Such a sheet can only exist when connected to another sheet but it is useful to calculate this mathematical problem in order to construct a realistic solution.) If γ is the strength of the vortex sheet in a strip defined by $u < x < \infty; u < y < \gamma$, then

$$|\boldsymbol{\gamma}| = Y \int |\boldsymbol{\omega}| \mathrm{d}\boldsymbol{n} = \frac{F_0}{U_0} \quad \text{where} \quad \boldsymbol{\omega} = (\omega_x, 0, 0). \tag{A 1}$$

Also, $\omega_x = \gamma\delta(z)$ and $\int_{-\infty}^{\infty} \omega_x \mathrm{d}z = \gamma$.

https://doi.org/10.1017/S0022112098001190 Published online by Cambridge University Press

Thence

$$z \to 0, u_y \to \gamma/2 \quad \text{for} \quad z > 0, \quad u_y \to -\gamma/2 \quad \text{for} \quad z < 0. \tag{A 2}$$

The velocity induced by the vortex sheet with strength $\boldsymbol{\gamma}$ is calculated from (Batchelor 1967, equation 2.68)

$$\boldsymbol{u} = \frac{1}{4\pi} \int \frac{\boldsymbol{\gamma} \times \boldsymbol{s}}{s^3} \mathrm{d}A(\boldsymbol{x}') \tag{A 3}$$

where $\boldsymbol{s} = (\boldsymbol{x} - \boldsymbol{x}', \boldsymbol{y} - \boldsymbol{y}', \boldsymbol{z} - \boldsymbol{z}')$. This gives

$$u_y = -\frac{1}{4\pi} \int_0^\infty \int_0^Y \frac{\gamma z \mathrm{d}x' \mathrm{d}y'}{[(x - x')^2 + (y - y')^2 + z^2]^{3/2}} \tag{A 4}$$

and

$$u_z = \frac{1}{4\pi} \int_0^\infty \int_0^Y \frac{\gamma (y - y') \mathrm{d}x' \mathrm{d}y'}{[(x - x')^2 + (y - y')^2 + z^2]^{3/2}}. \tag{A 5}$$

After simplification (and in the limit $Y \to \infty$)

$$u_y = +\frac{\gamma}{4\pi} \left(\tan^{-1} \frac{xy}{z(x^2 + y^2 + z^2)^{1/2}} + \tan^{-1} \frac{x}{z} + \tan^{-1} \frac{y}{z} + \tfrac{1}{2}\pi \right) \tag{A 6}$$

We note that as

$$x \to > 0, \quad y > 0, \quad z \to 0, \quad u_y \to \pm\gamma/2 \quad \text{for} \quad z \gtrless 0 \tag{A 7}$$

otherwise as $z \to 0$, outside the strip, $u_y = 0$. Also,

$$u_z = \frac{\gamma}{4_\pi} \left[-\sinh^{-1} \left(\frac{x}{((y - Y)^2 - z^2)^{1/2}} \right) + \sinh^{-1} \frac{x}{(y^2 + z^2)^{1/2}} + \ln \frac{((y - Y)^2 + z^2)}{y^2 + z^2} \right]. \tag{A 8}$$

Note that for $Y \ll |y| \ll x$ (for $x > 0$), $\boldsymbol{u}$ should tend to the solution for a line vortex of strength γY. Hence $u_z \sim -\gamma Y/(2\pi y)$, which agrees with (A 7).

REFERENCES

Abramovich, G. N. 1963 *The Theory of Turbulent Jets*. MIT Press.

Abramowitz, M. & Stegun, I. A. 1965 *Handbook of Mathematical Functions*. Dover.

Bache, D. H. & Johnstone, D. R. 1992 *Micro-climate and Spray Dispersion*. Ellis Horwood.

Bache, D. H. & Sayer, W. J. D. 1975 Transport of aerial spray. I. A model of aerial dispersion. *Agric. Met*. **15**, 257–271.

Batchelor, G. K. 1967 *An Introduction to Fluid Dynamics*. Cambridge University Press.

Briffa, F. F. J. & Dombrowski, N. 1966 Entrainment of air into a liquid spray. *AIChE J*. **12**, 708–717.

Castleman, R. A. 1931 The mechanism of atomization of liquids. *Bur. Stand. J. Res*. **6**, 369–376.

Coelho, S. L. V. & Hunt, J. C. R. 1989 The dynamics of the near-field of strong jets in cross-flows. *J. Fluid Mech*. **200**, 95–120.

Crowe, C. T., Sharma, M. P. & Stock, D. E. 1977 The particle source – in cell (psi-cell) model for gas-droplet flows. *Trans. ASME: J. Fluids Engng* **99** 325–332.

Dombrowski, N. & Frazer, R. P. 1953 A photographic investigation into the disintegration of liquid sheets. *Phil. Trans. R. Soc. Lond*. A **247**, 101–130.

Dombrowski, N. & Johns, W. R. 1963 The aerodynamic instability and disintegration of viscous sheets. *Chem. Engng Sci*. **18**, 203–214.

Dumbauld, N. J., Rafferty, J. E & Bjorkland, J. R. 1977 Prediction of spray behaviour above and within a forest canopy. *USDA Forest Service Rep*. TR-77-308-01.

Fuchs, N. A. 1964 *The Mechanics of Aerosols*. Pergamon.

https://doi.org/10.1017/S0022112098001190 Published online by Cambridge University Press

Ghosh, S. & Hunt, J. C. R. 1994 Induced air velocity in droplet-driven sprays. *Proc. R. Soc. Lond.* A **444**, 105–127.

Ghosh, S., Phillips, J. C. & Perkins, R. J. 1991 Modelling the flow in droplet driven sprays. In *Advances in Turbulence 3* (ed. A. V. Johansson & P. H. Alfredsson), pp. 405–413. Springer.

Goldschmidt, V. & Eskinazi, S. 1966 Two-phase turbulent flow in a plane jet. *J. Appl. Mech.* **33**, 735–747.

Hunt, J. C. R., Perkins, R. J. & Fung, J. C. H. 1994 Problems in modelling dispersed 2-phase flows. *Appl. Mech. Rev.* **47**, s49–s60.

Legg, B. J. & Raupach, M. R. 1982 Markov chain simulation of particle dispersion in inhomogeneous flows: the mean drift velocity induced by a gradient in Eulerian velocity variance. *Boundary-Layer Met.* **24**, 3–13.

Lee, S. Y. & Tankin, R. S. 1984 Study of liquid spray (water) in a non-condensable environment (air). *Intl J. Heat Mass Transfer* **27**, 351–361.

Miller, P. C. H. & Hadfield, D. J. 1989 A simulation of spray drift from hydraulic nozzles. *J. Agric. Engng. Res.* **42**, 135–147

Morton, B. R., Taylor, G. I. & Turner, J. S. 1956) Turbulent gravitational convection from maintained and instantaneous sources. *Proc. R. Soc. Lond.* A **234**, 1–23.

Perkins, R. J., Ghosh, S. & Phillips, J. C. 1991 Interaction of particles and coherent structures in a plane turbulent air jet. In *Advances in Turbulence 3* (ed. A. V. Johansson & P. H. Alfredsson pp. 93–100. Springer.

Phillips, J. C., Miller, P. C. H. & Thomas, N. H. 1998 An experimental investigation of the drift from agricultural boom sprayers. *Atomisation in Sprays* (to be submitted).

Picot, J. J. C., Kirstmanson, D. D. J. & Basak-Brown, N. 1986 Canopy deposit and off-target drift in forestry aerial spraying: the effect of operational parameters. *Trans. Am. Soc. Agric. Engng* **29**, 80–88.

Schweitzer, P. H. 1937 The mechanism of disintegration of liquid jets. *J. Appl. Phys.* **8**, 513–521.

Smith, S. H. & Mungal, M. G. 1998 Mixing, structure and scaling of the jet in cross-flow. *J. Fluid Mech.* **357**, 83–122.

Squire, H. B. 1953 Investigation of instability of a moving liquid film. *Brit. J. Appl. Phys.* **4**, 167–172.

Sykes, R. I., Lewellen, W. S. & Parker, S. F. 1986 On the vorticity dynamics of a turbulent jet in a cross-flow. *J. Fluid Mech.* **168**, 393–413.

Taylor, G. I. 1944 Air resistance of a flat plate of very porous material. *Aero. Res. Counc. A & M* 2236. Reprinted in *Scientific Papers of G. I. Taylor* (ed. G. K. Batchelor) 1963, pp. 383–386. Cambridge University Press.

Taylor, G. I. 1958 Flow induced by jets. *J. Aero. Space Sci.* **25**, 464–465.

Thompson, N. J. & Ley, A. J. 1983 Estimating spray drift using a random walk model of evaporating drops. *J. Agric. Engng Res.* **28**, 418–435.

Walklate, P. J. 1987 A random-walk model for dispersion of heavy particles in turbulent air flow. *Boundary-Layer Met.* **39**, 175–190.

Wallis, G. B. 1969 *One-Dimensional Two-Phase Flows.* McGraw-Hill.

https://doi.org/10.1017/S0022112098001190 Published online by Cambridge University Press